JACS
JOURNAL OF THE AMERICAN CHEMICAL SOCIETY
Article
pubs.acs.org/JACS

Nonclassical Crystal Growth as Explanation for the Riddle of Polarity in Centrosymmetric Glycine Crystals

Elena Meirzadeh,[†,∥] Liel Sapir,[§,∥] Hagai Cohen,[‡] Sidney R. Cohen,[‡] David Ehre,[†] Daniel Harries,[*,§] Meir Lahav,[*,†] and Igor Lubomirsky[*,†]

[†]Department of Materials and Interfaces and [‡]Department of Chemical Research Support, Weizmann Institute of Science, Rehovot 76100, Israel

[§]Institute of Chemistry and The Fritz Haber Research Center, The Hebrew University, Jerusalem 91904, Israel

ABSTRACT: The riddle of anomalous polar behavior of the centrosymmetric crystal of α-glycine is resolved by the discovery of a polar, several hundred nanometer thick hydrated layer, created at the {010} faces during crystal growth. This layer was detected by two independent pyroelectric analytical methods: (i) periodic temperature change technique (Chynoweth) at ambient conditions and (ii) contactless X-ray photoelectron spectroscopy under ultrahigh vacuum. The total polarization of the surface layer is extremely large, yielding $\approx$1 μC·cm^{-2}, and is preserved in ultrahigh vacuum, but disappears upon heating to 100 °C. Molecular dynamics simulations corroborate the formation of polar hydrated layers at the sub-microsecond time scale, however with a thickness of only several nanometers, not several hundred. This inconsistency might be reconciled by invoking a three-step nonclassical crystal growth mechanism comprising (i) docking of clusters from the supersaturated solution onto the evolving crystal, (ii) surface recognition and polar induction, and (iii) annealing and dehydration, followed by site-selective recrystallization.

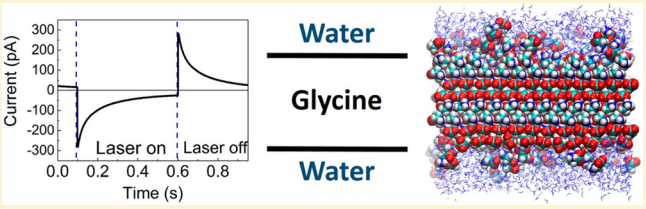

INTRODUCTION

Pyroelectricity is the development of surface charge created at the hemihedral faces of polar crystals upon temperature variation.[1] This property is confined exclusively to the polar directions of the 10 polar crystalline classes.[2] Coster et al.[3] and Cooke et al.[4] investigated scintillations (electric discharge) and current pulses, occurring upon heating and cooling of polar crystals. In their studies, the centrosymmetric crystals of α-glycine were used as a distinctive nonpolar reference system.[5] In contrast to their expectations, they observed electric discharge also from those nonpolar crystals. In order to clarify the origin of this unusual effect, they further investigated the properties of these crystals and reported anomalous temperature dependence of conductance and capacitance, providing additional support for anomalous pyroelectricity from an apparently centrosymmetric crystal.[3] Such pyroelectricity could imply either the presence of structural disorder or contamination by one of the other two polar, β or γ, polymorphs of glycine. Langan et al.,[6] however, invalidated experimentally these two suppositions by performing meticulous neutron diffraction studies of the α-glycine crystals at different temperatures. They did not detect any disorder or chemical contamination that would lead to polarity. Therefore, the anomalous pyroelectric effect could not originate from the crystalline matrix. More recently, as part of our studies on the mechanism of symmetry reduction in doped organic crystals,[7] we found independently surface pyroelectricity in nonpolar crystals of amino acids.[8,9]

Here we provide a rational explanation for the anomalous polar behavior of the centrosymmetric crystals of α-glycine, by applying pyroelectric measurements, X-ray photoelectron spectroscopy (XPS)-based measurements,[10,11] atomic force microscopy (AFM), and molecular dynamics (MD) simulations. We discovered the formation of very thick polar layers during crystal growth, on the two {010} enantiotopic faces, that display unusually large surface charge of the same sign. The surface charge reaches $\approx$1 μC·cm^{-2}, comparable to strongly polar materials like $BaTiO_3$ and $PbTiO_3$.[12] Consequently, the large surface charge might potentially affect the properties and the functionality of materials, as already described for glycine,[3−5] and influence processes such as crystal growth, catalysis and adhesion, to mention but a few. In particular, these findings provide experimental support for the "nonclassical" crystal growth mechanism.[13−16] It is shown that clusters created in supersaturated solutions may attach to the surfaces of the growing crystals, and assume a polar configuration thereby becoming detectable by the pyroelectric measurements. Consequently, such clusters play a role not only in the early stages of crystal nucleation, as required by the "nonclassical" nucleation mechanism, but also in the ensuing process of crystal growth.

RESULTS

Pyroelectricity was examined in the following systems:

Received: September 4, 2016
Published: October 13, 2016

DOI: 10.1021/jacs.6b09190
J. Am. Chem. Soc. 2016, 138, 14756−14763

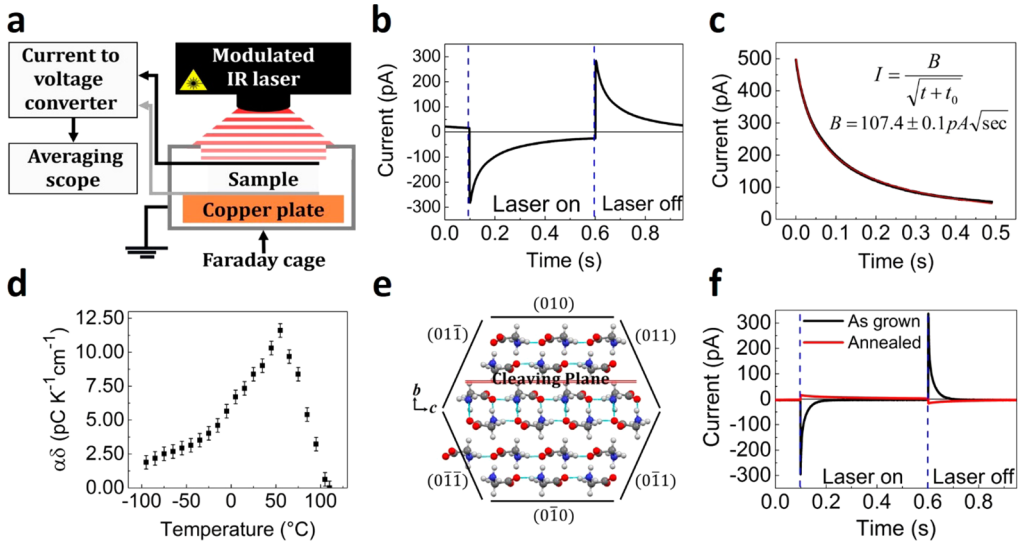

Figure 1. Pyroelectric measurement via periodic-temperature-change technique. (a) Illustration of the experimental setup. (b) Pyroelectric current, from (010) surface of α-glycine crystal, as a function of heating and cooling cycles. (c) Fitting of the current vs time dependence. (d) SPCP as a function of surrounding temperature. (e) α-glycine packing arrangement, showing the cleaving plane. (f) Pyroelectric signal of α-glycine crystal doped with *L*-threonine before and after annealing.

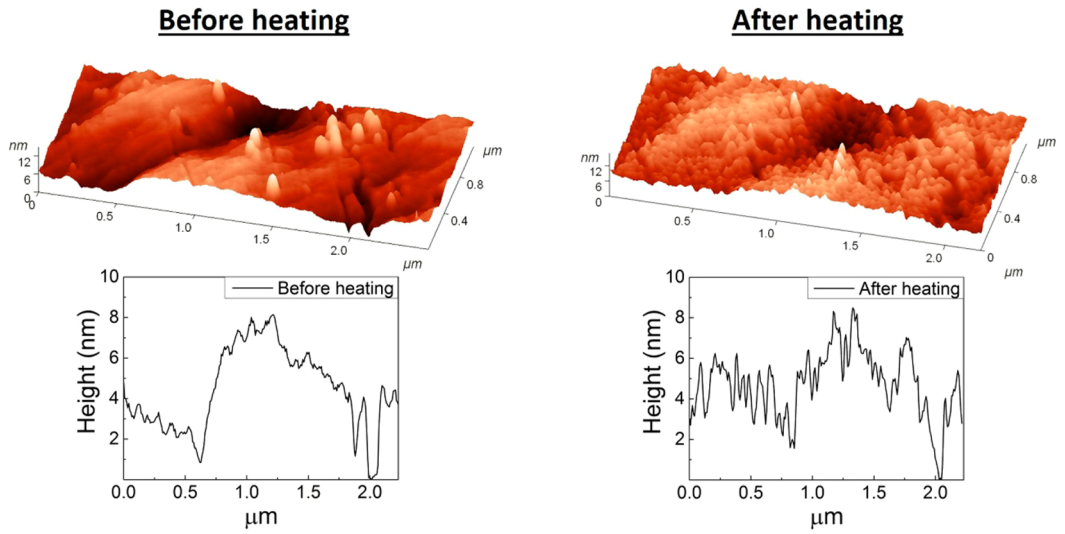

Figure 2. Surface reconstruction of a fresh (010) face of α-glycine. AFM measurement before and after heating to ≈100 °C for 1 h. Image size 2.2 × 1 μm^2, with height scale of 12 nm. Typical cross section profiles are shown below the images.

(a) α-Glycine crystals as-grown in aqueous solutions, which exhibit surface pyroelectricity.
(b) Cleaved α-glycine crystals, as references lacking pyroelectricity.
(c) Annealed α-glycine crystals doped with *L*-threonine, as references that display bulk pyroelectricity: The doping reduces the symmetry of the glycine crystal, which gives rise to relatively weak bulk polarization and pyroelectricity,[17] whereas annealing at 100 °C eliminates the surface pyroelectricity only.
(d) As-grown α-glycine crystals doped with *L*-threonine that show both surface and bulk pyroelectricity.

Periodic Temperature Change Technique. The surface pyroelectricity was measured by the modified Chynoweth[18] method (Figure 1a), which is based on measurement of the transient current upon rapid heating. The current from the two {010} enantiotopic faces of the as-grown pure α-glycine crystals is negative upon heating and decays sharply a few milliseconds after switching the heating laser on (Figure 1b). Since the thickness of the pyroelectric layer, δ, cannot be determined from the electrical measurement, the surface pyroelectric coefficient, $\alpha_S \equiv \partial P_s/\partial T$ (where P_s is the near surface polarization and T the temperature) cannot be calculated directly. However, the surface pyroelectric coefficient product (SPCP), defined as $\alpha_s\delta$, is assessable and, for all practical purposes, can serve as a measure of the surface pyroelectricity. The SPCP is given by:[18]

$$\mathrm{SPCP} = \alpha_S\delta = \frac{B(d+\delta)C_v\sqrt{\pi D}}{F_d A_c} \quad (1)$$

where d is the thickness of the crystal, C_v is the thermal capacitance per unit volume, D is the heat diffusion coefficient, F_d is the heat flux at the surface, and A_c is the contact area. As the thickness of the polar layer is negligible, $\delta \ll d$, δ can be

DOI: 10.1021/jacs.6b09190
J. Am. Chem. Soc. 2016, 138, 14756−14763

Table 1. Surface Pyroelectric Coefficient Product, SPCP, $\alpha_s\delta$, of a Single α-Glycine Crystal, Broken into Two Pieces, One Measured at Ambient Environment and the Other in Ultrahigh Vacuum

crystal state	$\alpha_s\delta$ in ambient environment ($C\cdot cm^{-1}\cdot K^{-1}$)	$\alpha_s\delta$ in ultrahigh vacuum ($C\cdot cm^{-1}\cdot K^{-1}$)
fresh crystal	$(1.81 \pm 0.05) \times 10^{-11}$	$(1.74 \pm 0.05) \times 10^{-11}$
after 4 h	$(1.52 \pm 0.05) \times 10^{-11}$	$(1.48 \pm 0.05) \times 10^{-11}$
after 12 h	$(1.48 \pm 0.05) \times 10^{-11}$	$(1.48 \pm 0.05) \times 10^{-11}$
after 72 h	$(1.10 \pm 0.05) \times 10^{-11}$	$(1.11 \pm 0.05) \times 10^{-11}$

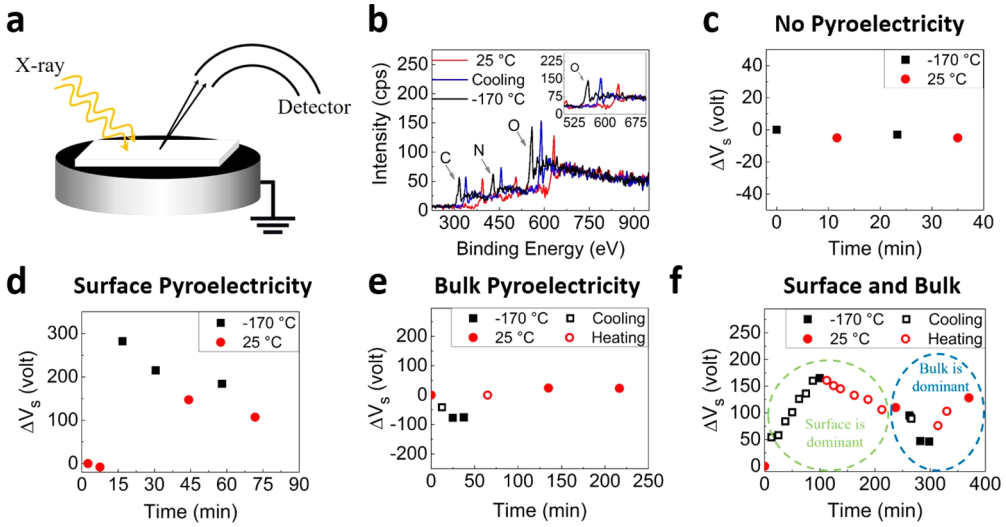

Figure 3. Contact-free pyroelectric measurements using XPS. (a) Illustration of the experimental setup. (b) Spectra demonstrating peak shifts upon cooling the annealed *L*-threonine doped glycine, inset: Zoomed view of the O 1s peaks. Scanning is from right to left and differences between the shifts of different lines are due to the continuous cooling over the course of the scan. Note that the changes in binding energies do not correspond to changes in oxidation states, but rather to the global surface potential. (c–f) Changes in the surface potential, ΔV_s, with temperature vs irradiation time, where ΔV_s refers to the deviation from the initial potential at $t = 0$. (c) Cleaved α-glycine; the cycled change in temperature does not affect V_s. (d) As grown α-glycine crystal; note the V_s increase/decrease upon cooling/heating and the gradual suppression of ΔV_s upon increased exposure to the beam. (e) Annealed *L*-threonine doped α-glycine; here V_s reversibly decreases/increases upon cooling/heating. (f) As-grown *L*-threonine doped α-glycine; consisting of both surface and bulk pyroelectricity. In (c) and (d), measurements (exposure to X-rays) were taken only after temperature stabilization. In (e)–(f), measurements were taken continuously along the heating/cooling cycles.

neglected in eq 1. The value of B can be extracted from the time dependence of the pyroelectric current, I (Figure 1c):[18]

$$I = \frac{B}{\sqrt{t + t_0}} \tag{2}$$

The SPCP value obtained for the as-grown crystals at room temperature is $(1.4 \pm 0.4) \times 10^{-11}$ $C\cdot cm^{-1}\cdot K^{-1}$. It increases reversibly with temperature up to ≈60 °C, and then decreases irreversibly until it completely disappears at ≈100 °C (Figure 1d). Heating the crystal also results in substantial surface roughening and reconstruction, as verified by AFM measurements (Figure 2). Interestingly, the SPCP value decreases to ≈60% of its original value after 3 days (Table 1). This decay is insensitive to whether the crystals are kept at ambient conditions or under ultrahigh vacuum.

The molecularly smooth[19] cleaved (010) face, which exposes the C_α–H bonds (Figure 1e), does not exhibit surface pyroelectricity. However, surface pyroelectricity appears after the cleaved face has been dipped into water. Its SPCP at room temperature is ≈30 times smaller than that of the as-grown face: $(5 \pm 2) \times 10^{-13}$ vs $(1.4 \pm 0.4) \times 10^{-11}$ $C\cdot cm^{-1}\cdot K^{-1}$.

Since the pyroelectric coefficient is defined as the temperature derivative of polarization, the values of $P_s\delta$ at different temperatures can be estimated by integrating $\alpha_s\delta$, from the relevant temperature, up to the temperature at which it disappears, $T_{\max(\alpha\to 0)}$ (Figure 1d). Values of the product $P_s\delta$ as a function of temperature for as-grown and cleaved-and-dipped crystals are plotted in Figure 7d,e.

Our data show that the surface pyroelectricity of *L*-threonine doped glycine crystals is of opposite sign and larger in magnitude compared to that of the bulk, as seen by comparing the pyroelectric response of the same samples as-grown and after annealing them at 100 °C for 1 h (Figure 1f). Independently, the bulk pyroelectric coefficient of the annealed crystals was derived from the average current value,[20] yielding:

$$\alpha_B = \frac{IC_v d}{F_d A} = -(1.3 \pm 0.5) \times 10^{-11}\ C\cdot cm^{-2}\cdot K^{-1} \tag{3}$$

Contact-Free Pyroelectric Measurements by XPS. In contrast to the Chynoweth method that measures the derivative of the polarization with temperature, $\partial P_s/\partial T$, XPS measures the average change in polarization over a temperature range $\Delta P_s/\Delta T$ by probing directly the surface potential, V_s.

The kinetic energy, E_k, of electrons emitted from a material under monochromatic X-ray irradiation (Figure 3a,b) is determined from the condition for energy conservation:

$$E_k = h\upsilon - E_B - \phi + eV_s \tag{4}$$

where $h\upsilon$ is the photon energy, E_B is the binding energy of the atomic orbital from which the electron was emitted, ϕ is the spectrometer work-function[21] and e is the elementary electric charge. One can estimate the pyroelectric coefficient from

DOI: 10.1021/jacs.6b09190
J. Am. Chem. Soc. 2016, 138, 14756–14763

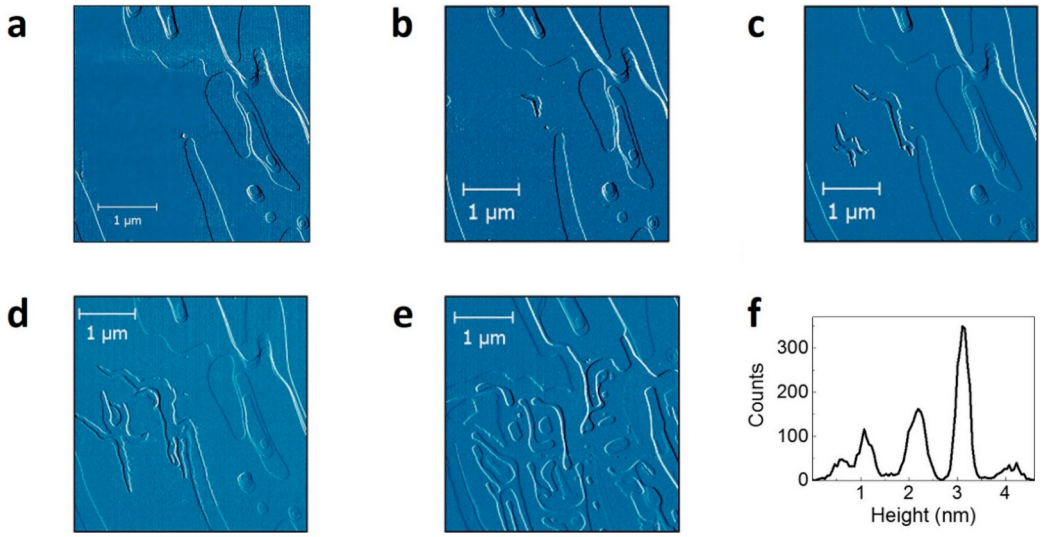

Figure 4. AFM observations of spontaneous roughening of the (010) face of α-glycine in ≈70% humidity (in order to highlight the surface changes, error signal rather than height signal is presented). (a) Freshly cleaved crystal, (b–e) after 40 min, 2.5 h, 3 h, and 5 h (respectively). (f) Histogram of the step heights of the rough surface. Image size 4 × 4 μm^2.

changes in V_s (ΔV_s), by measuring the changes in E_k, as long as only the spontaneous polarization is temperature dependent. The pyroelectric coefficient of a bulk polar crystal, α_B, can be expressed approximately as[11] $\alpha_B = \frac{\Delta V_s \varepsilon \varepsilon_0}{d\Delta T}$, where ε is the dielectric constant of the sample, ε_0 is the vacuum permittivity, and d is the sample thickness. Similarly, the surface pyroelectric coefficient, α_s, is described as $\alpha_s = \frac{\Delta V_s \varepsilon \varepsilon_0}{\delta \Delta T}$, where δ is the thickness of the pyroelectric layer. Positive ΔV_s is defined here to represent an increase in the surface electrostatic energy, hence an increase in E_k.

The temperature-induced variations in surface potential were recorded here between −170 and +25 °C. As anticipated, in the case of the cleaved α-glycine crystal, no variations in surface potential were observed upon repeated cooling/heating cycles (Figure 3c). On the other hand, the surface potential of as-grown pure glycine crystals increased by ≈300 V under the first cooling cycle (Figure 3d). The corresponding SPCP value of the as-grown α-glycine is $(1.5 \pm 0.1) \times 10^{-12}$ C·cm^{-1}·K^{-1}. Consistently, the X-ray irradiation resulted in a gradual decrease of the total surface potential. Sequential measurements at a fixed temperature clearly exemplify this degradation, as manifested by the two data points at 17 and 30 min in Figure 3d.

The annealed *L*-threonine doped glycine exhibits only bulk pyroelectricity. In fact, the bulk effect is expressed by surface potential changes of ≈100 V upon cooling and heating, yielding $\alpha_B = (1.2 \pm 0.1) \times 10^{-11}$ C·cm^{-2}·K^{-1} and retaining remarkable stability under the X-ray irradiation (Figure 3e), in contrast to the instability of surface pyroelectricity.

Finally, we examine the coexistence of surface and bulk pyroelectricity by inspecting the as-grown *L*-threonine doped glycine. Figure 3f shows an initial increase by ≈+170 V upon cooling, which demonstrates that the surface effect is dominant, in agreement with the periodic-temperature-change technique results (Figure 1f). At the limit of very long exposures, >5 h, corresponding to effective elimination of the surface signal, the total signal stabilizes at ≈−85 V. Consequently, the detected magnitudes of surface and bulk pyroelectricity in this sample are each in line with the results obtained from the previous samples: ≈+300 V for the surface only (recall that at 100 min there is already partial degradation in the surface component) and close to −100 V for the bulk only. Further details of the gradual change in relative magnitudes, surface vs bulk, can be seen in Figure 3f. In particular, the crossover regime, with comparable surface and bulk magnitudes, occurs only at the end of the first cooling–heating cycle (after ≈20 min exposure to X-ray irradiation, Figure 3f). Accordingly, upon further cooling, the sign of ΔV_s becomes opposite to the sign detected at the beginning of this experiment and, as seen in the last four data points, Figure 3f, the full heating step stabilizes eventually on a 85 V change in the surface potential. Thus, the surface vs bulk polarizations were successfully differentiated.

In Situ AFM Measurements under Humid Environment. The atomically smooth, cleaved (010) face was examined by AFM at room temperature and ≈70% humidity. Forty minutes after cleaving the crystal, a spontaneous surface roughening was detected (seen as a new feature appearing in the middle of the image of Figure 4b). This roughening increases with time (Figure 4), while the individual step heights remain compatible with integer multiples of half the *b*-axis in the α-glycine unit cell[6] (b = 11.9 Å): 6 Å, 11 Å, 22 Å, 32 and 44 Å (Figure 4f). The surface energy can be estimated by the relation $T_c \approx ula/k_B$, where T_c is the critical surface reconstruction temperature, u is the surface energy per unit area, l is a typical footprint of a molecule, $1 < a < 2$ is a constant depending on the number of surface sites that can accommodate one molecule and k_B is the Boltzmann constant. The spontaneous surface roughening (at room temperature) indicates that T_c < 300 K, hence the surface energy of the (010) face in the presence of water vapor is necessarily <20 mJ·m^{-2}, which is an extremely low value for solids, approaching that of fluorinated hydrocarbon surfaces.[22]

Molecular Dynamics Simulations. In order to assess the perturbation induced by water on the crystal structure, and the possible role of this perturbation on the pyroelectric properties of the crystal, we analyzed molecular dynamics (MD) simulations of an initially molecularly flat α-glycine crystal, wetted by a water layer that is ≈1.5 nm thick. The crystal is oriented so that the hydrophilic {010} faces are orthogonal to

DOI: 10.1021/jacs.6b09190
J. Am. Chem. Soc. 2016, 138, 14756–14763

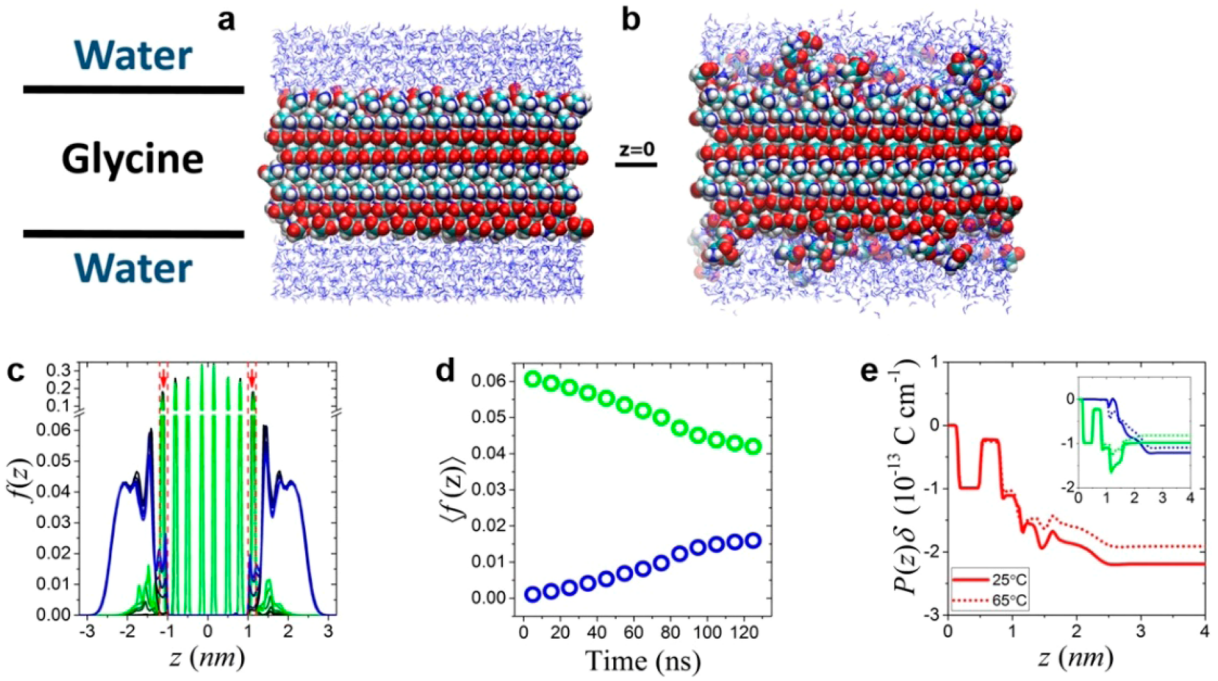

Figure 5. Water-induced alterations to α-glycine crystal with initial flat hydrophilic {010} surfaces. (a) Glycine plus water system before interaction. (b) The steady-state configuration after water has perturbed the surface (for 100 ns). (c) The probability density at T = 298 K for water (blue) and glycine (green) molecules along the $\hat{z}$ axis, $f(z)$, where the origin is set at the center of the crystal. Different curves represent progressing times along the simulation trajectory from the first 10 ns (darkest color) to the last 10 ns (lightest) from a 130 ns long trajectory. (d) Time evolution of the probability density for water (blue) and glycine (green) molecules at distances $1< |z| < 1.2$ nm (between the indicated dashed red lines in panel c). (e) The cumulative dipole per surface area (related to the spontaneous polarization, see text for details), $P_s(z)\delta$, as a function of the vertical distance z. Inset: Dissected contributions of water (blue) and glycine (green) to $P_s(z)$.

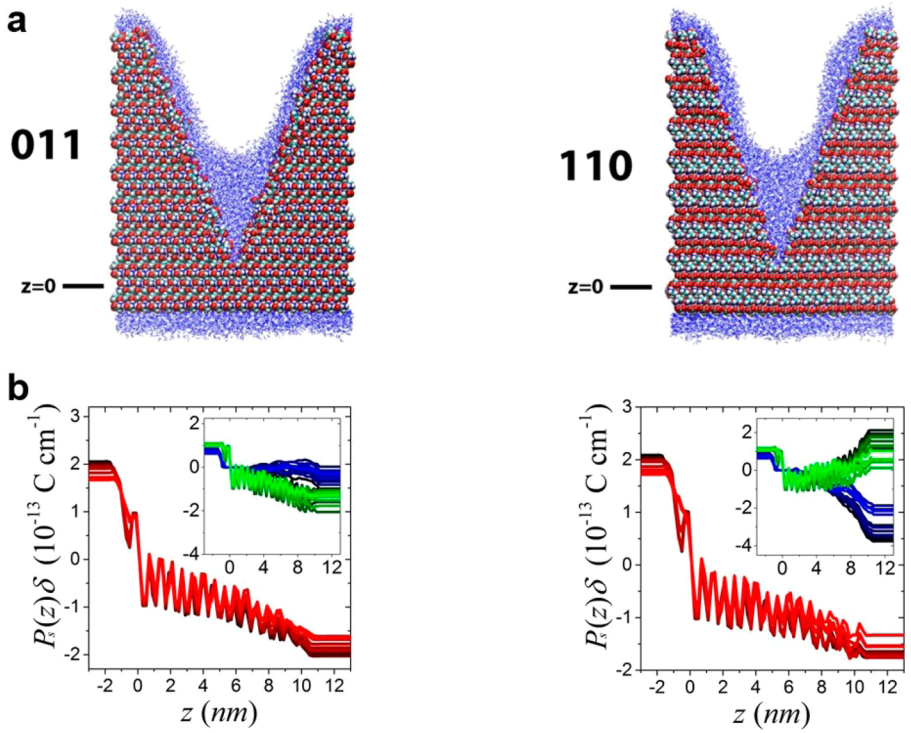

Figure 6. Emergence of near surface pyroelectricity in MD simulations of a wetted α-glycine crystal with crevices presenting the {011}, {110} and the flat hydrophobic {010} faces (at the bottom of the crevices). (a) Snapshot of the simulation box, where water molecules are colored blue and the glycine molecules are in the vdW representation. (b) Cumulative dipole per surface area, $P_s(z)\delta$ (see eq 5), as a function of the vertical distance z. Inset: Dissected contributions of water (blue) and glycine (green) to $P_s(z)$. The different curves represent temperatures ranging from 273 K (darkest color) to 372 K (lightest).

DOI: 10.1021/jacs.6b09190
J. Am. Chem. Soc. 2016, 138, 14756−14763

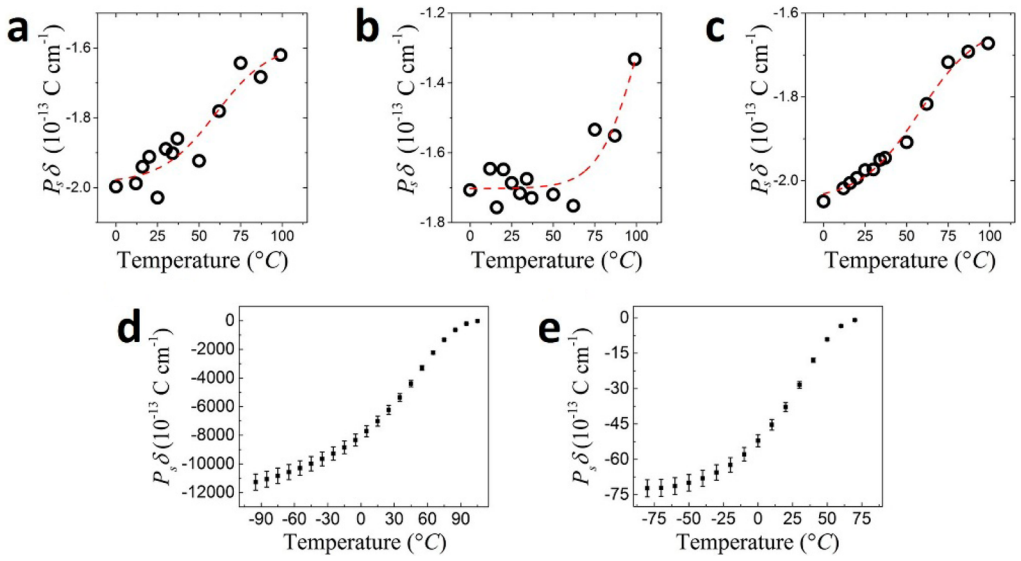

Figure 7. Temperature dependence of the cumulative dipole per surface area, $P_s(z)\delta$. (a–c) Asymptotic value of the spontaneous polarization from the MD simulations as a function of temperature, for the {011} crevice facet (a), the {110} crevice faces (b), and the flat {010} hydrophobic faces (c). Red dashed lines are guides for the eye. (d,e) Experimental values for the as-grown and the cleaved-and-dipped {010} faces, respectively.

the $\hat{z}$ axis, and the origin ($z = 0$) is set at the center of the crystal slab (Figure 5a,b). As also known for other facets of glycine crystals,[23] over the 130 ns time-course of the simulation, water molecules penetrate the crystal, then deform and reconstruct its surface, Figure 5c. This dynamic process suggests that when these faces of the centrosymmetric crystal are wetted, the symmetry is reduced, thus resulting in net dipole accumulation. Our simulations further show that the spontaneous polarization of the (initially) flat layer (calculated as described in the following) is temperature-dependent (Figure 5d). These findings suggest a possible mechanism by which water perturbs and restructures the surface of the glycine crystal. Given that such surface modifications can take place, we next examined the molecular properties of a crystal that already contains a large interfacial defect in the form of a crevice (Figure 6a).

The spontaneous polarization, P_s, at each distance along the $\hat{z}$ axis in terms of the total cumulative dipole per surface area is:[24]

$$P_s(z)\delta = A_{xy}^{-1} \sum_{z} \mu_{\hat{z}} \tag{5}$$

where A_{xy} is the cross-sectional area of the simulation box, orthogonal to $\hat{z}$, $\mu_{\hat{z}}$ is the $\hat{z}$-component of each molecular dipole, and $\delta = |z|$. The summation in eq 5 was performed in the positive and negative directions of $\hat{z}$ relative to $z = 0$. Values of $P_s(z)\delta$ for a range of temperatures are plotted for both crevices in Figure 6b. This quantity can be further dissected into the separate contributions of the glycine and water dipoles (Figure 6b, insets).

We finally evaluated the asymptotic value of the cumulative dipole (i.e., the value of $P_s(z)\delta$ for large z) in terms of the spontaneous polarization at the crevice facet, and examined its temperature dependence, Figure 7. For both types of crevices, the absolute value of $P_s\delta$ decreases with temperature (Figure 7a,b). The same analysis was also performed on the flat (010) hydrophobic face at the underside of the crevice, Figure 7c, suggesting that without a crevice the spontaneous polarization has even stronger temperature dependence.

DISCUSSION

The presence of a near surface polar layer, formed at the two {010} faces during growth of α-glycine in aqueous solution, has been detected by two independent methods: the modified Chynoweth technique at ambient conditions, and a contactless XPS method in ultrahigh vacuum. Both methods yield similar values of the pyroelectric coefficient: $SPCP_{(Chynoweth)} = (2.0 \pm 0.5) \times 10^{-12}$ vs $SPCP_{(XPS)} = (1.5 \pm 0.1) \times 10^{-12}$ C·cm^{-1}·K^{-1} as measured around −100 °C. The two techniques strongly differ in the exposure to compensating ambient ions. In addition, the Chynoweth technique inspects time derivatives, whereas XPS probes the electrostatic potential, providing the (steady-state) surface charge.[10] Thus, the close agreement between the two methods excludes possible artifacts such as surface modification upon electrode attachment.[11]

Both methods confirm that the dry surfaces of glycine, obtained by crystal cleavage, do not display pyroelectricity. Moreover, the appearance of surface pyroelectricity upon dipping a cleaved crystal in water confirms that the polarity is linked to the interaction of glycine with water.

Our MD simulations imply that wetting induces the formation of a mixed hydrated polar layer composed of glycine molecules, distorted from their crystallographic sites in the crystals and interacting through their zwitterions with the water molecules (Figure 5). This dynamic process can modify the topology of the crystal faces by creating defects and crevices (Figure 6). However, the value of $P_s\delta$ (averaged over the different faces at 0 °C) as deduced from the MD simulations is $(1.9 \pm 0.2) \times 10^{-13}$ C·cm^{-1}, which is 30 times smaller than that of experimentally cleaved-and-dipped crystals $(5.5 \pm 0.2) \times 10^{-12}$ C·cm^{-1}, and more than 4000 times smaller than the value for as-grown crystals $(8.9 \pm 0.05) \times 10^{-10}$ C·cm^{-1}. Such differences in $P_s\delta$ values cannot be explained by considering only differences in the polarization values. Rather, our simulations were performed at the submillisecond time-scale and considered only a limited number of hydrating water molecules, thus allowing only minor perturbations to the crystal surface. Nonetheless, the MD simulations show the existence of the surface rearrangement, within the computational limi-

DOI: 10.1021/jacs.6b09190
J. Am. Chem. Soc. 2016, 138, 14756–14763

tations. Therefore, it is reasonable that the effective thickness of the polar layer in the experiment is much larger than in the simulations (at least $\delta \approx 100$ nm vs $\approx$1−2 nm). Assuming such thicknesses, the effective polarization of the surface layer is still very high, $P_s \approx 1\ \mu C \cdot cm^{-2}$, which is quite surprising, since this value compares well with strongly polar materials, like $BaTiO_3$ or $PbTiO_3$.[12] For a more moderate P_s the effective thickness should necessarily be even larger to fit our observations.

In order to provide a possible explanation for the formation of such thick polar layers we consider nonclassical nucleation and crystal growth mechanisms,[13−16,25,26] in which the nucleus is formed by the coalescence of clusters present in the supersaturated solution. These clusters can even form well below the supersaturated regime, as was shown for other small molecules.[27,28] Studies of dissolution of glycine have demonstrated that ≈250 nm "liquidlike" glycine-rich hydrated clusters are formed.[29] In addition, the evolution and structural properties of polar open dimers of glycine, and longer head-to-tail oligomers have been observed by SAXS studies, further supported by MD simulations, to form stable and abundant aggregates present in supersaturated solutions.[30−32] We suggest that in our system such hydrated clusters and glycine molecules may coalesce and attach to the {010} faces of the growing crystal by a process of surface recognition. Similar surface recognition and enantiomeric crystal segregations was suggested in the crystal growth of sodium bromate.[33]

The sense of polarity of the attached hydrated clusters might be induced either by the polar hydrated surface of the crystal nuclei, as suggested by the MD simulations (Figure 5), or by the screw dislocations propagating along the *b*-direction of the crystals.[34] As previously suggested in other systems, the mobility of such clusters or crystallites may be quite high and their reorientation should be relatively fast.[35,36] The surface energy deduced from the AFM measurements, showing spontaneous roughening, is very low. Therefore, the driving force for surface reconstruction is also very low. This fact explains the long-term stability of the surface polar layer.

The glycine crystals doped with *L*-threonine display both bulk polarity and surface polarity. Appearance of the bulk polarity demands strictly stereospecific incorporation of the *L*-threonine molecules, while the surface polarity indicates nonclassical crystal growth. Thus, presence of both surface and bulk pyroelectricity implies that the nonclassical crystal growth mechanism preserves stereospecificity. This conclusion is in full agreement with the earlier described mechanism of occlusion of "tailor-made" auxiliaries in doped crystals.[17,37,38] It also implies that, after the attachment, the clusters undergo site-selective structural transformation, involving the removal of any hydrated capping layer.

CONCLUSIONS

Our results suggest that two conditions are necessary in order to observe large surface polarity: (i) the nonclassical crystal growth mechanism leading to the formation of a polar surface layer and (ii) low surface energy, which makes it stable for a sufficiently long time to be detected. Since all surfaces that delineate crystals are polar, we may anticipate polarity to be observed in other inorganic and organic systems as well. Thus, pyroelectric measurements combined with MD simulations can provide structural information regarding these surfaces. Moreover, such studies may provide insights regarding the different mechanisms of crystallization. Future directed experiments as well as simulations on a longer time scale should be able to test such mechanisms. Applications of the present methods to other systems are under current investigation.

MATERIALS AND METHODS

Crystal Growth. Pure and mixed crystals of α-glycine were grown by slow evaporation method in a clean room environment from aqueous solutions at 23 °C. A supersaturated (130%) pure glycine solution and glycine (Alfa Aesar 99.5+%) in the presence of 5 wt %·wt^{-1} *L*-threonine (T-Fisher Scientific 99.0−101.0%) were prepared by dissolving the amino acids in water (Ultrapure Millipore water, 18.2 MΩ cm at 25 °C, Millipore Synergy UV, Type 1 water), and heating it to ≈80 °C to achieve full dissolution. The solutions were filtered through cotton wool into glass crystallization growth dishes which were covered with filter paper to facilitate slow evaporation. Large transparent single crystals were chosen, washed in water and dried. The crystalline structure was verified and the major faces of the crystals were indexed with Ultima-III (sealed X-ray tube, Cu anode, 3 kW, RIGAKU, Japan) X-ray diffractometer. The presence of crystallites of the polar β- or γ- polymorphs were excluded. In addition, meticulous neutron diffraction[6] could not detect other crystalline phases rather than the centrosymmetric α-glycine polymorph.

MD Simulations. We simulated two types of molecular systems. The first consisted of molecularly smooth hydrophilicly terminated {010} faces of the α-glycine crystal comprising 12 × 12 × 2 unit cells and wetted by 2692 water molecules (Figure 5a). The second type of simulation consisted of α-glycine crystals containing a large crevice, exposing either the {011} or {110} faces to the solution (Figure 6a). These simulation boxes consisted of 8720 glycine molecules and 8580 water molecules, each.

All simulations were performed with the GROMACS package,[39−42] using the OPLS-AA force-field[43] and the TIP4P water model.[44] The simulation boxes were prepared with an expanded void layer on both sides of the wetted crystalline. The simulations were performed in the isobaric-isothermic ensemble (appropriate for an isolated crystal) at various temperatures and at a pressure of P = 1 atm. Temperatures were held constant using the Nosé−Hoover thermostat with a 1 ps coupling constant.[45,46] Pressure was kept using the Parrinello−Rahman barostat with a 1 ps coupling constant.[47,48] Electrostatic calculations were performed using the particle-mesh Ewald (PME) method with 1 Å grid spacing and a pseudo-2D summation.[49,50] Periodic boundary conditions were used throughout with a time-step of 2 fs, and all bond lengths to hydrogen atoms were kept constant with the LINCS algorithm.[51] van der Waals interactions were truncated smoothly with a switching distance of 10 Å and a cutoff distance of 12 Å, while accounting for long-range dispersion corrections. After a short equilibration step, the flat slabs were simulated for 130 ns at 298 K, while the crevices were simulated for at least 50 ns at different temperatures over the range [273−372 K].

AFM Measurements. AFM measurements were made on an NT-MDT NTEGRA (Zelenograd, Ru) with SU005 head and sample scanner, with range of approximately 80 × 80 μm^2. The measurements were made in semicontact mode using an Olympus AC160 probe with resonance frequency of 335 kHz.

XPS Measurements. The measurements were performed on a Kratos AXIS-Ultra DLD spectrometer, using an extremely low X-ray source power, 0.3 W, and detection pass energy of 80 eV. Base pressure at the analysis chamber was 5×10^{-10} Torr. Due to the severe problem of charging in these samples, each analysis was complemented by repeated scans prior and post temperature change that allowed reliable elimination of the beam induced charging effects. Successful elimination of this artifact is achieved upon stabilization of the potential, as demonstrated in Figure 3c, where pyroelectric effects do not interfere, as well as by sequential data points at a fixed temperature in Figure 3e. A coldfinger liquid nitrogen cooling was used to decrease the temperature at the back side of the sample holder. The samples rose to room temperature after stopping the nitrogen flow. To verify the stabilization of surface temperature we performed two types of complementary measurements: (1) A continuous follow-up: For each temperature step, repeated scans were performed until the surface

DOI: 10.1021/jacs.6b09190
J. Am. Chem. Soc. 2016, 138, 14756−14763

potential stabilized. Note the finer time-scale information allowed by distinct spectral signals within the broad scan (see Figure 3b). (2) A minimized irradiation mode: Making every temperature change without exposure to the X-ray radiation and allowing a long stabilization time (up to an hour, as deduced from the previous measurements) prior to the acquisition of a new spectroscopic scan. Complementary chemical analyses were performed at 15 W and detection pass energy of 20 eV, using an electron flood gun for surface potential stabilization. Beam induced charging effects were eliminated by introducing repeated measurements with a detailed follow-up of time dependencies, all performed at extremely low source power, ≤0.2 W.

AUTHOR INFORMATION

Corresponding Authors

*daniel.harries@mail.huji.ac.il
*meir.lahav@weizmann.ac.il
*igor.lubomirsky@weizmann.ac.il

Author Contributions

‖E.M. and L.S. contributed equally.

Notes

The authors declare no competing financial interest.

ACKNOWLEDGMENTS

The manuscript is dedicated to Prof. Ben Feringa. The authors thank Dr. Isabelle Weissbuch (Weizmann Institute) for helpful discussions and express their appreciation to the Israeli Science Foundation and Perlman fellowship. This research is made possible in part by the historic generosity of the Harold Perlman Family. L.S. is supported by the Adams Fellowship Program of the Israel Academy of Sciences and Humanities. The Fritz Haber Research Center is supported by the Minerva Foundation, Munich, Germany. Funding was provided by The Israeli Science Foundation (226/13), Perlman fellowship and the Adams Fellowship Program of the Israel Academy of Sciences and Humanities

REFERENCES

(1) Lang, S. B. *Phys. Today* **2005**, *58*, 31.
(2) Kittel, C. *Introduction to solid state physics*; Wiley: New York, 2005.
(3) Chilcott, T. C.; Schoenborn, B. P.; Cooke, D. W.; Coster, H. G. L. *Philos. Mag. B* **1999**, *79*, 1695.
(4) Cooke, D. W.; Khan, S. M.; Alexander, C. *Phys. Rev. B: Condens. Matter Mater. Phys.* **1980**, *21*, 4166.
(5) Cooke, D. W.; Alexander, C. *Phys. Rev. B* **1976**, *14*, 1333.
(6) Langan, P.; Mason, S. A.; Myles, D.; Schoenborn, B. P. *Acta Crystallogr., Sect. B: Struct. Sci.* **2002**, *58*, 728.
(7) Vaida, M.; Shimon, L. J. W.; Weisinger-Lewin, Y.; Frolow, F.; Lahav, M.; Leiserowitz, L.; McMullan, R. K. *Science* **1988**, *241*, 1475.
(8) Piperno, S.; Mirzadeh, E.; Mishuk, E.; Ehre, D.; Cohen, S.; Eisenstein, M.; Lahav, M.; Lubomirsky, I. *Angew. Chem., Int. Ed.* **2013**, *52*, 6513.
(9) Mishuk, E.; Weissbuch, I.; Lahav, M.; Lubomirsky, I. *Cryst. Growth Des.* **2014**, *14*, 3839.
(10) Cohen, H. *Appl. Phys. Lett.* **2004**, *85*, 1271.
(11) Ehre, D.; Cohen, H. *Appl. Phys. Lett.* **2013**, *103*, 052901.
(12) Von Hippel, A. *Rev. Mod. Phys.* **1950**, *22*, 221.
(13) Ivanov, V. K.; Fedorov, P. P.; Baranchikov, A. Y. e.; Osiko, V. V. e. *Russ. Chem. Rev.* **2014**, *83*, 1204.
(14) Vorontsova, M. A.; Maes, D.; Vekilov, P. G. *Faraday Discuss.* **2015**, *179*, 27.
(15) Niederberger, M.; Colfen, H. *Phys. Chem. Chem. Phys.* **2006**, *8*, 3271.
(16) De Yoreo, J. J.; Gilbert, P. U.; Sommerdijk, N. A.; Penn, R. L.; Whitelam, S.; Joester, D.; Zhang, H.; Rimer, J. D.; Navrotsky, A.; Banfield, J. F.; et al. *Science* **2015**, *349*, aaa6760.
(17) Meirzadeh, E.; Azuri, I.; Ehre, D.; Rappe, A. M.; Lahav, M.; Kronik, L.; Lubomirsky, I. *Nat. Commun.* **2016**, *7*, 13351.
(18) Ehre, D.; Mirzadeh, E.; Stafsudd, O.; Lubomirsky, I. *Ferroelectrics* **2014**, *472*, 41.
(19) Gidalevitz, D.; Feidenhans'l, R.; Matlis, S.; Smilgies, D. M.; Christensen, M. J.; Leiserowitz, L. *Angew. Chem., Int. Ed. Engl.* **1997**, *36*, 955.
(20) Lubomirsky, I.; Stafsudd, O. *Rev. Sci. Instrum.* **2012**, *83*, 051101.
(21) Seah, M. P.; Briggs, D. *Practical Surface Analysis: Auger and X-ray Photoelectron Spectroscopy*; John Wiley & Sons: New York, 1990.
(22) Tokuda, K.; Ogino, T.; Kotera, M.; Nishino, T. *Polym. J.* **2015**, *47*, 66.
(23) Banerjee, S.; Briesen, H. *J. Chem. Phys.* **2009**, *131*, 184705.
(24) Peng, Q.; Cohen, R. E. *Phys. Rev. B: Condens. Matter Mater. Phys.* **2011**, *83*, 220103.
(25) Li, D. S.; Nielsen, M. H.; Lee, J. R. I.; Frandsen, C.; Banfield, J. F.; De Yoreo, J. J. *Science* **2012**, *336*, 1014.
(26) Ectors, P.; Sae-Tang, W.; Chatchawalsaisin, J.; Zahn, D.; Anwar, J. *Cryst. Growth Des.* **2015**, *15*, 4026.
(27) Sapir, L.; Harries, D. *J. Phys. Chem. B* **2011**, *115*, 624.
(28) Lerbret, A.; Bordat, P.; Affouard, F.; Descamps, M.; Migliardo, F. *J. Phys. Chem. B* **2005**, *109*, 11046.
(29) Jawor-Baczynska, A.; Sefcik, J.; Moore, B. D. *Cryst. Growth Des.* **2013**, *13*, 470.
(30) Hamad, S.; Hughes, C. E.; Catlow, C. R. A.; Harris, K. D. M. *J. Phys. Chem. B* **2008**, *112*, 7280.
(31) Yani, Y.; Chow, P. S.; Tan, R. B. H. *Cryst. Growth Des.* **2012**, *12*, 4771.
(32) Erdemir, D.; Chattopadhyay, S.; Guo, L.; Ilavsky, J.; Amenitsch, H.; Segre, C. U.; Myerson, A. S. *Phys. Rev. Lett.* **2007**, *99*, 115702.
(33) Viedma, C.; McBride, J. M.; Kahr, B.; Cintas, P. *Angew. Chem., Int. Ed.* **2013**, *52*, 10545.
(34) Shtukenberg, A. G.; Zhu, Z. N.; An, Z. H.; Bhandari, M.; Song, P. C.; Kahr, B.; Ward, M. D. *Proc. Natl. Acad. Sci. U. S. A.* **2013**, *110*, 17195.
(35) Henning, C.; Vermaak, J. *Appl. Phys. Lett.* **1969**, *15*, 3.
(36) Pikin, S.; Vlasov, V. *Kristallografiya* **1992**, *37*, 1303.
(37) Weissbuch, I.; Addadi, L.; Lahav, M.; Leiserowitz, L. *Science* **1991**, *253*, 637.
(38) Belitzky, A.; Weissbuch, I.; Posner-Diskin, Y.; Lahav, M.; Lubomirsky, I. *Cryst. Growth Des.* **2015**, *15*, 2445.
(39) Hess, B.; Kutzner, C.; van der Spoel, D.; Lindahl, E. *J. Chem. Theory Comput.* **2008**, *4*, 435.
(40) Van der Spoel, D.; Lindahl, E.; Hess, B.; Groenhof, G.; Mark, A. E.; Berendsen, H. J. C. *J. Comput. Chem.* **2005**, *26*, 1701.
(41) Lindahl, E.; Hess, B.; van der Spoel, D. *J. Mol. Model.* **2001**, *7*, 306.
(42) Berendsen, H. J. C.; van der Spoel, D.; van Drunen, R. *Comput. Phys. Commun.* **1995**, *91*, 43.
(43) Jorgensen, W. L.; Maxwell, D. S.; TiradoRives, J. *J. Am. Chem. Soc.* **1996**, *118*, 11225.
(44) Jorgensen, W. L.; Chandrasekhar, J.; Madura, J. D.; Impey, R. W.; Klein, M. L. *J. Chem. Phys.* **1983**, *79*, 926.
(45) Nose, S. *Mol. Phys.* **1984**, *52*, 255.
(46) Hoover, W. G. *Phys. Rev. A: At., Mol., Opt. Phys.* **1985**, *31*, 1695.
(47) Parrinello, M.; Rahman, A. *J. Appl. Phys.* **1981**, *52*, 7182.
(48) Nosé, S.; Klein, M. *Mol. Phys.* **1983**, *50*, 1055.
(49) Darden, T.; York, D.; Pedersen, L. *J. Chem. Phys.* **1993**, *98*, 10089.
(50) Essmann, U.; Perera, L.; Berkowitz, M. L.; Darden, T.; Lee, H.; Pedersen, L. G. *J. Chem. Phys.* **1995**, *103*, 8577.
(51) Hess, B.; Bekker, H.; Berendsen, H. J. C.; Fraaije, J. G. E. M. *J. Comput. Chem.* **1997**, *18*, 1463.

DOI: 10.1021/jacs.6b09190
J. Am. Chem. Soc. 2016, 138, 14756−14763